Virtual Synchronous Machine-based Control of a Single-phase Bi-directional Battery Charger for Providing Vehicle-to-Grid Services

Jon Are Suul, *Member IEEE*, Salvatore D'Arco and Giuseppe Guidi, *Member IEEE*

***Abstract* – This paper presents a single-phase Virtual Synchronous Machine (VSM) and its possible application for providing Vehicle-to-Grid (V2G) services from domestic battery chargers of Electric Vehicles (EVs). In a VSM, the power converter is controlled to emulate the inertia and the damping effect of a synchronous machine. Thus, a VSM-based EV charger can contribute to the spinning reserve and the frequency regulation of the power system. In case of grid outages, the VSM can seamlessly establish an islanded grid and supply local loads from the battery onboard the EV. In order to avoid the influence on the virtual inertia from power oscillations associated with a single phase circuit, the proposed control scheme relies on a virtual two-phase system for calculating active and reactive powers. The proposed VSM implementation is described in detail and its dynamic performances in grid-connected as well as stand-alone operation are demonstrated by numerical simulations and by laboratory experiments.**

***Index Terms*—Bidirectional Battery Charger, Electric Vehicle Charging, Vehicle-to-Grid Services, Virtual Synchronous Machine**

I. Introduction

Increasing availability of Electric Vehicles (EVs) and a correspondingly wider selection of models from the car manufacturers are resulting in increased sales of EVs. Technological advances leading to continuously improving performances, and in particular increasing energy density, of Li-Ion batteries are also leading to a growing energy capacity of the onboard EV battery storage systems, ranging from around 20 kWh for the middle class segment to over 80 kWh for high class models. Although the share of EVs within the private transportation sector is still limited on a global scale, political price incentives have shown to significantly impact the sales. For example, as a result of such incentives, more than 15% of all passenger cars sold in Norway in 2015 had batteries as their only energy source for propulsion [1]. Considering also Plug-in hybrid Electric Vehicles (PHEV), the total market share of passenger cars with possibility for battery charging from the power system was exceeding 20 % in 2015 [1]. Thus, in regions with high shares of EVs and PHEVs, the local penetration of domestic EV chargers is expected to increase towards levels where their operation can have significant impact on the power system. This might lead to a need for ancillary services and a corresponding market where it can be beneficial to provide Vehicle-to-Grid (V2G) functionality from EV chargers [2], [3].

Domestic EV chargers can be designed and controlled to provide several basic V2G services, like voltage control or reactive power control, frequency-dependent power regulation and load shifting [4]. Furthermore, controllability of active and reactive power implies that EV chargers can also contribute to stabilization of power or voltage oscillations in the grid. From a general power system perspective, EVs connected to the grid through their chargers do not only represent a load, but also a potential distributed storage system. Indeed, some of the stored energy in the EV batteries can be made available to the grid if bi-directional chargers are adopted. This can allow for additional V2G functionalities, including inertia emulation with transient power injection from the battery to the grid in case of sudden frequency transients due to loss of generation or other power system faults. Furthermore, the energy from the EV battery can be used to supply small local loads like individual households in islanded operation, even for several hours, in case of power outages in the main grid [5]- [7].

A promising control approach for providing distributed ancillary services from power electronic converters is to apply the concept of Virtual Synchronous Machines (VSMs) [8]-[13]. Such control approaches can inherently ensure inertia emulation and frequency support as well as local reactive power or voltage control. Although the VSM concept was originally proposed for applications in renewable and distributed generation systems, provision of ancillary services from VSM-controlled EV chargers has also been discussed [14]-[17]. However, except for [16], [18], previously proposed methods for VSM-based control have focused on three-phase power converters while most domestic EV chargers are single-phase systems.

If a VSM implementation designed for three-phase systems is directly applied to a single-phase converter, its virtual inertia will experience the same power or torque oscillations as a physical single-phase machine. Thus, it will

Manuscript received July 30, 2015; revised December 18, 2015; accepted March 3, 2016. Paper 2015-IPCC-700.R1, presented at the 9th International Conference on Power Electronics – ECCE Asia, Seoul, Korea, June 1–5 2015, and approved for publication in the IEEE Transactions on Industry Applications by the Industrial Power Converter Committee of the IEEE Industry Applications Society. The work of SINTEF Energy Research in this paper was supported by the project "Releasing the Potential of Virtual Synchronous Machines–ReViSM" through the Blue Sky instrument of SINTEF Energy Research as a Strategic Institute Programme (SIP) financed by the national Basic Funding Scheme of Norway.

J. A. Suul is with the Department of Electric Power Engineering, Norwegian University of Science and Technology, 7495 Trondheim, Norway, and also with SINTEF Energy Research, 7465 Trondheim, Norway, jon.are.suul@ntnu.no

S. D'Arco and G. Guidi are with SINTEF Energy Research, 7465 Trondheim, Norway, salvatore.darco@sintef.no, giuseppe.guidi@sintef.no

Color versions of one or more of the figures in this paper are available online at http://ieeexplore.ieee.org.

Digital Object Identifier

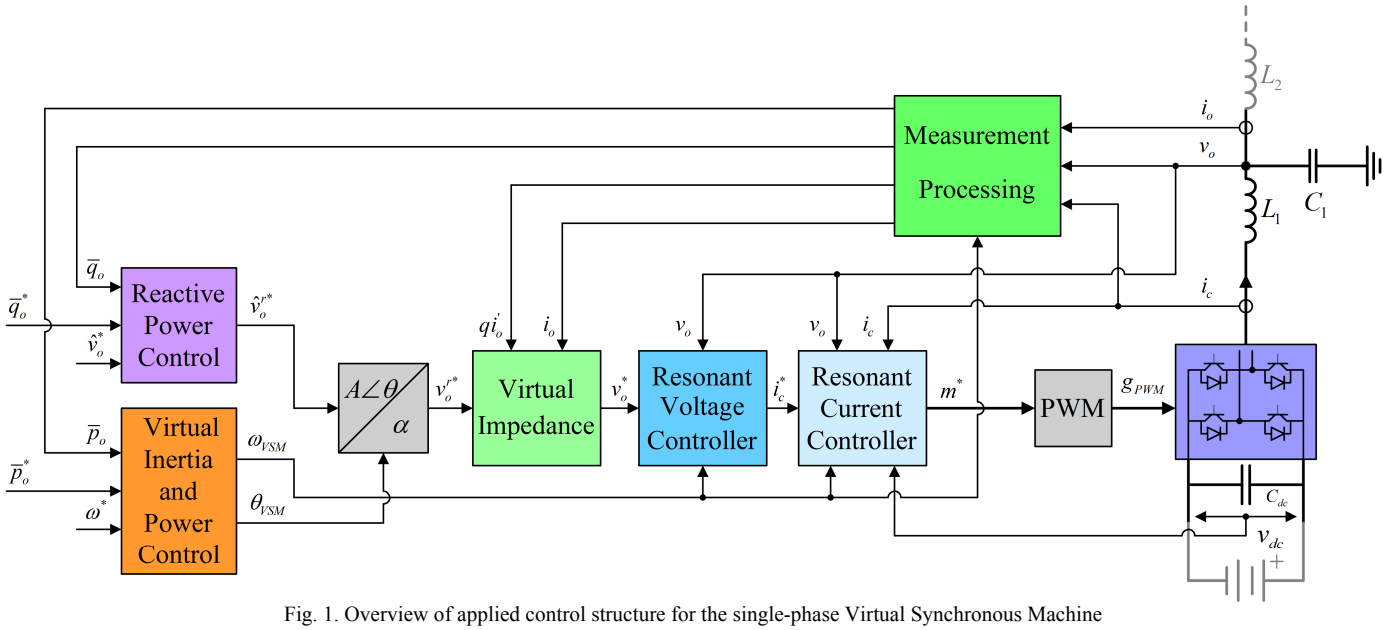

Fig. 1. Overview of applied control structure for the single-phase Virtual Synchronous Machine

be necessary with a large inertia that will be continuously exposed to double frequency power oscillations. However, this can be avoided by establishing a virtual two-phase system for calculating the VSM active and reactive power flow, as proposed in [16] and [18]. Thus, the inertia emulation of a single-phase VSM can be designed with equivalent parameters and performances as corresponding three-phase implementations. Two different proposals for implementing this approach have been previously proposed in [16] and [18], but without any experimental verification. This paper, which is an extended version of [19], presents a further improvement of the single-phase VSM structure from [16], when operated as an EV battery charger. All elements of the applied VSM implementation are described in detail, and the performances are verified by both time domain simulations and laboratory experiments. In particular, the presented results demonstrate the intended performance in grid connected operation as well as for sudden islanding with a local load fed from the EV-battery.

II. Control System for a Single-Phase Virtual Synchronous Machine

An overview of the applied control scheme for the single-phase VSM is shown in Fig. 1, where the functional blocks and their signal interfaces are highlighted.

A. Overview of system configuration

For the investigated case, the power circuit consists of a single-phase H-bridge converter connected to the grid through an LC- or LCL-filter, as indicated in the right side of Fig. 1. The dc side capacitor of the converter is assumed to be connected to an EV battery, although the same scheme could also be used for any other controllable source or load. Sensors are assumed to be present for measuring the dc bus voltage v_{dc}, the output current of the converter i_c, the filter capacitor voltage v_o and the output current i_o from the LC filter. Upper case symbols shown in the electrical circuit indicate physical quantities, while lower case symbols indicate per unit quantities used in the control system. Reference values for any given signal x are indicated by a superscript asterisk as x^*.

The control scheme presents three layers of cascaded controllers:

i. An inner loop current controller provides the modulation index m^* for the Pulse Width Modulation (PWM) of the converter output voltage.
ii. A voltage controller regulates the filter capacitor voltage by providing the current reference for the inner loop current controller.
iii. The outer layer features active and reactive power controllers emulating the main characteristics of Synchronous Machine (SM) behavior.

The voltage reference resulting from the reactive power control loop and the phase angle resulting from the power control with SM emulation are combined into a sinusoidal voltage reference. The voltage drop across a virtual impedance is subtracted from this sinusoidal voltage reference before it is used to control the filter capacitor voltage. Furthermore, the block labelled as "Measurement Processing" in Fig. 1 includes the generation of a virtual two-phase system used for calculating the active and reactive power feedback signals used by the outer control loops. The implementation of these control functions are described in the following subsections.

B. Cascaded voltage and current resonant controllers

The internal structures of the voltage and current control loops applied in the presented VSM scheme are shown in Fig. 2, with the current controller to the left. In this case, a proportional-resonant (PR) controller is applied to track the sinusoidal current reference i_c^* without steady-state errors, and the corresponding continuous time transfer functions are given in the figure [20], [21]. Frequency-adaptive operation of the PR controller is ensured by applying a Second Order Generalized Integrator (SOGI) according to [21] for the resonant term. The current controller proportional and integral gains are denoted by k_{pc} and k_{ic} respectively, while a

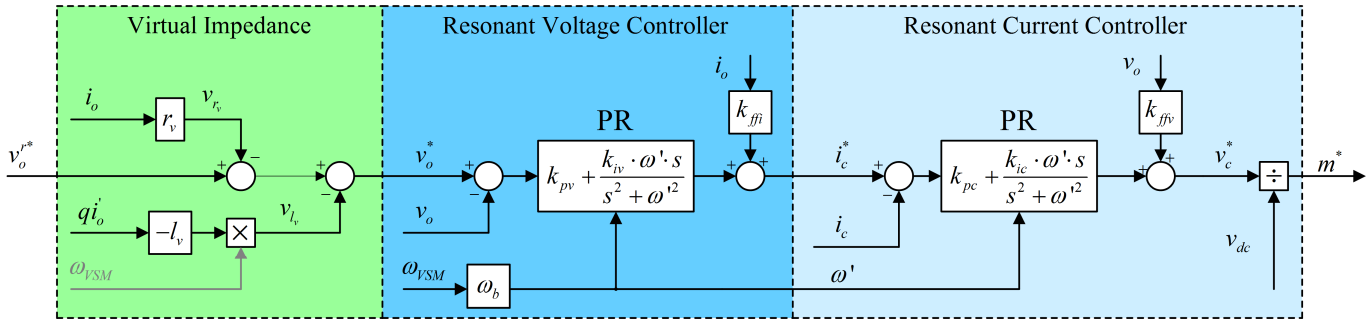

Fig. 2. Cascaded voltage and current control based on frequency-adaptive PR controllers with Virtual Impedance acting on the voltage reference

feed-forward path for the measured capacitor voltage can be enabled or disabled by setting the parameter k_{ffv} to 1 or 0. The modulation index m^* is calculated by dividing the voltage reference v_c^* by the measured dc voltage v_{dc}, to avoid a nonlinear relation between the voltage reference and the converter output voltage. With voltage feed-forward enabled, this implies that the open loop transfer function for the current controller can be expressed by (1).

$$h_{cc}(s) = \underbrace{\left(k_{pc} + k_{ic}\frac{\omega' \cdot s}{s^2 + \omega'^2}\right)}_{\text{PR-controller}} \cdot \underbrace{\frac{1}{1 + T_d \cdot s}}_{\text{Delay approximation}} \cdot \underbrace{\frac{1}{r_{L_1}}\frac{1}{1 + T_{L_1} \cdot s}}_{\text{Filter inductor}} \quad (1)$$

Assuming relatively high switching frequency of the converter, the PR current controller can be tuned according to its equivalence with a PI current controller in the synchronous reference frame [22]. Thus, simple tuning rules as discussed in [23] can be used as starting point for the controller design.

The voltage controller tracks the capacitor voltage reference v_o^* by generating the current reference for the inner loop current controller. The same type of PR controller as described for the current controller is assumed, with k_{pv} and k_{iv} representing the proportional and integral gains. Under the same assumptions as for the current controller, the open loop transfer function of the voltage controller can be expressed by (2).

$$h_{vc}(s) = \underbrace{\left(k_{pv} + k_{iv}\frac{\omega' \cdot s}{s^2 + \omega'^2}\right)}_{\text{PR-controller}} \cdot \underbrace{\frac{h_{cc}(s)}{1 + h_{cc}(s)}}_{\text{Closed loop cc}} \cdot \underbrace{\frac{1}{T_C \cdot s}}_{\text{Filter capacitor}} \quad (2)$$

Similar types of tuning considerations as for the current controller can be applied also to the voltage control loop. However, the pure integral effect and the corresponding −90° initial phase of the filter capacitor frequency characteristics must be taken into account, and sufficient bandwidth separation between the current and voltage control loops must be ensured. As demonstrated for a three-phase converter in [24], this approach is reasonable for high switching frequencies, but will not necessarily be reliable if the sampling and switching frequencies are below the range of 5-10 kHz. As domestic EV chargers operate with power levels of a few kW, they are usually designed with relatively high switching frequency to reduce volume and to avoid audible noise. Thus, challenges for tuning of cascaded PR controllers at low switching and sampling frequencies will not be further considered.

C. Virtual impedance

As shown in Fig. 1, the sinusoidal voltage reference v_o^{r*} is calculated from the amplitude and phase angle provided by the outer loops for active and reactive power control:

$$v_o^{r*} = \hat{v}_o^{r*}\cos(\theta_{VSM}) \quad (3)$$

where $\hat{v}_o^{r*}$ is the voltage amplitude reference from the reactive power control loop and θ_{VSM} is the phase angle resulting from the emulation of the SM swing equation. The capacitor voltage reference v_o^* is then obtained by subtracting a voltage drop associated with a virtual impedance from v_o^{r*}, as given by (4)

$$v_o^* = v_o^{r*} - \underbrace{(r_v + j \cdot \omega_{VSM} \cdot l_v) \cdot i_0}_{v_{r_v} + v_{l_v}} \quad (4)$$

This virtual impedance can be considered as a quasi-stationary equivalent of the stator impedance of a SM. Therefore, v_o^{r*} will correspond to the internal induced voltage of a SM. However, the amplitude and phase of the capacitor voltage reference tracked by the voltage control loop will also depend on the output current i_o. As a result, the capacitor voltage v_o will be controlled to a value equivalent to the terminal voltage of an SM. Since the converter is operating with a PR capacitor voltage controller, this approach is necessary for ensuring stable operation in case of a strong grid or in case of direct parallel operation of multiple VSM units. Operation with predominantly inductive virtual impedance will also improve the VSM power angle regulation mechanism the same way as discussed for a three-phase VSM in [13].

As indicated in (4) and to the left of Fig. 2, the resistive voltage drop is calculated by multiplying i_o by the virtual resistance r_v. However, the direct calculation of the voltage drop in a virtual inductor would imply the use of differentiation, which again might cause high frequency noise that must be attenuated with low-pass filters [25]. To avoid the phase shift and amplitude attenuation associated with low pass filtering, a quasi-stationary approximation as proposed in [26] is instead applied to calculate the virtual inductive voltage drop:

$$v_{l_v} = l_v \omega_{VSM} \cdot (-qi_o') \approx l_v \cdot (-qi_o') \quad (5)$$

where qi'_o is a filtered in-quadrature (i.e. 90° delayed) version of the output current i_o, while l_v is the virtual inductance. The per unit angular frequency of the VSM is given by ω_{VSM}, but as long as limited frequency variations are expected, the frequency dependence of the virtual impedance

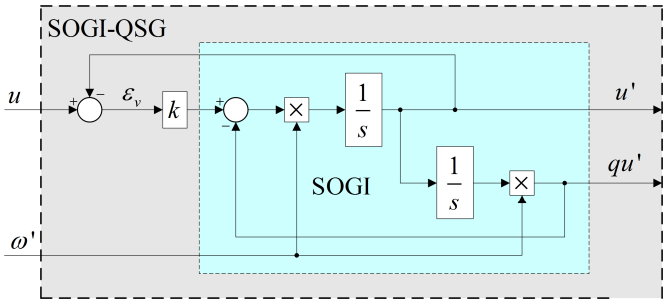

Fig. 3. Second Order Generalized Integrator (SOGI) configured as a Quadrature Signal Generator (QSG)

can be ignored in the implementation (i.e. $\omega_{VSM} \approx 1.0$ p.u.). The approach in (5) is based on the assumption that the derivative of the current during quasi-stationary conditions is equal in amplitude but opposite in phase (i.e. 180° shifted) to the in-quadrature current. The generation of the in-quadrature current component will be discussed in the following subsection.

D. Generation of a virtual two phase system

The challenges related to single-phase grid synchronization are commonly addressed by generating a virtual two phase system where the traditional techniques from three-phase systems like Synchronous Reference Frame (SRF) Phase Locked Loops (PLLs) and voltage vector oriented control can be applied [27]. However, for VSM-based control, the synchronization mechanism is integrated with the power balance of a virtual swing equation [12]. Thus, the challenges of single-phase VSM implementations can be addressed by estimating the dynamic average value of the active and reactive power flows, $\bar{p}$ and $\bar{q}$, and using these signals as feedback for the outer loop controllers as indicated in Fig. 1 [16].

The estimation of average active and reactive power needed for a single-phase VSM can be easily implemented in a virtual two-phase system. A set of Second Order Generalized Integrators (SOGIs) configured as Quadrature Signal Generators (QSGs), with a structure as shown for a generic signal u in Fig. 3, can be applied for this purpose [16], [18], [21]. The SOGI-QSGs are in this case used to generate in-quadrature signals (qv'_0 and qi'_o) corresponding to the filtered single-phase output voltage and current (v'_0 and i'_o), as given on generic form by:

$$\frac{u'(s)}{u(s)} = \frac{k \cdot \omega' \cdot s}{s^2 + k \cdot \omega' \cdot s + \omega'^2}$$
$$\frac{qu'(s)}{u(s)} = \frac{k \cdot \omega'^2}{s^2 + k \cdot \omega' \cdot s + \omega'^2} \quad (6)$$

Since the signals u' and qu' will be 90° phase shifted in stationary conditions, a virtual two-phase orthogonal vector representation can be established for the voltage measurements as well as for the current measurements by applying the same filtering technique, as shown in Fig. 4. In this virtual two-phase system, the vector amplitudes of the currents and voltages are equal to the amplitude of the measured single-phase currents and voltages respectively. Thus, the per unit active and reactive powers in this virtual two-phase system can be calculated directly according to:

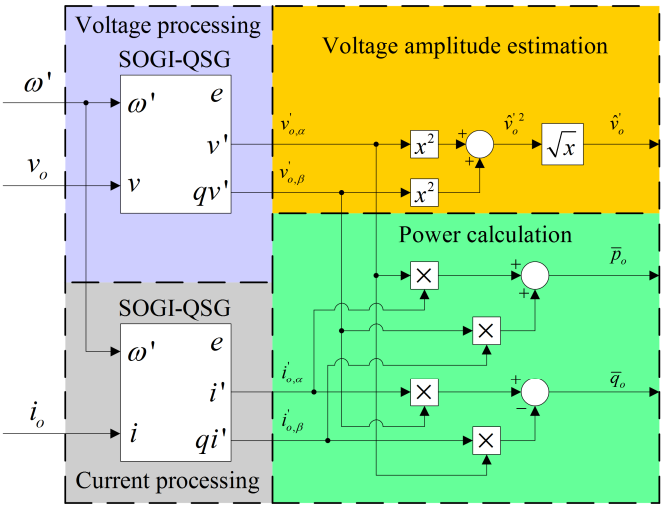

Fig. 4. Processing of single phase measurements for calculation of average active and reactive power and single phase signal amplitudes

$$\bar{p}_o = v'_{o,\alpha} \cdot i'_{o,\alpha} + v'_{o,\beta} \cdot i'_{o,\beta}$$
$$\bar{q}_o = v'_{o,\beta} \cdot i'_{o,\alpha} - v'_{o,\alpha} \cdot i'_{o,\beta} \quad (7)$$

This calculation, as also indicated to the lower right of Fig. 4, will correspond to the dynamic average values of the active and reactive power flows in the actual single-phase physical system. The voltage and current amplitudes can also be calculated directly from the virtual two phase system as shown for the output voltage amplitude to the upper right of Fig. 4.

E. Active and reactive power controllers

The active power control with the power-balance-based grid synchronization is the core of the VSM implementation since it ensures the emulation of the SM inertial behavior. Indeed, the proposed implementation is based on a simplified swing equation which models the inertia and the damping of a SM as discussed in [12]. This swing equation for the single-phase implementation can be expressed by:

$$s \cdot \omega_{VSM} \approx \frac{1}{T_a}\left[\bar{p}_o^{*} - \bar{p}_o - k_d\left(\omega_{VSM} - \omega_g\right)\right] \quad (8)$$

The detailed implementation of the VSM inertia and power control loop, including a power-frequency droop function acting on the power reference, is shown in Fig. 5. In the schematic, the steady state frequency droop gain is given by k_ω while k_d represents the damping coefficient of the VSM inertia and T_a is the inertia time constant (corresponding to $2H$ in a synchronous machine). The per unit angular frequency ω_{VSM} of the virtual inertia results directly from the power balance of the VSM swing equation in (8). This frequency is integrated to obtain the instantaneous phase angle θ_{VSM} needed for transforming the voltage amplitude reference into a sinusoidal voltage reference. Thus, the grid synchronization of the single-phase VSM is based entirely on the power balance calculated from the dynamic average value of the output power from (7).

The damping term on the virtual inertia emulates the effect of the damper windings of a SM, and is according to (8) given by the damping coefficient k_d and the difference between the VSM speed and the actual grid frequency. The latter is not directly available to the control system, although

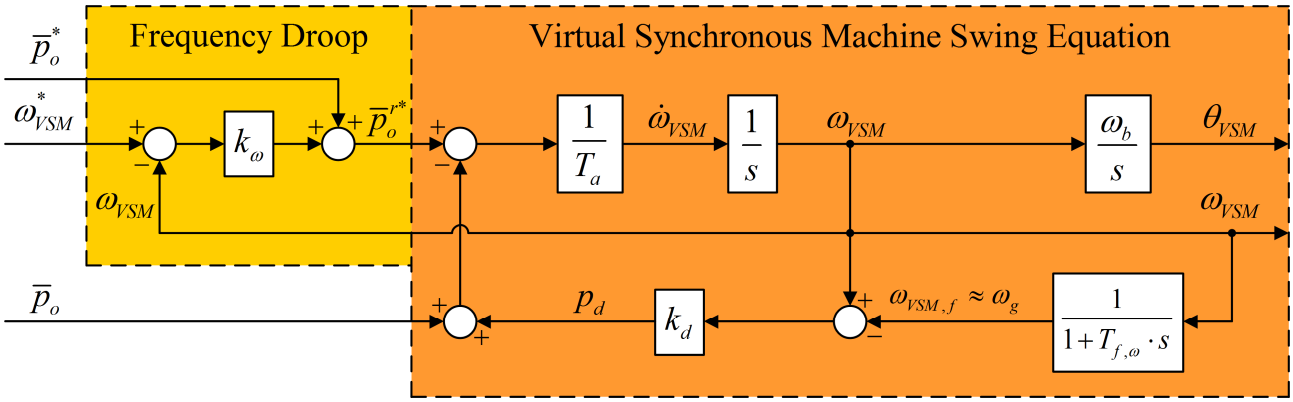

Fig. 5. Virtual Synchronous Machine swing equation with power-frequency droop on the power reference

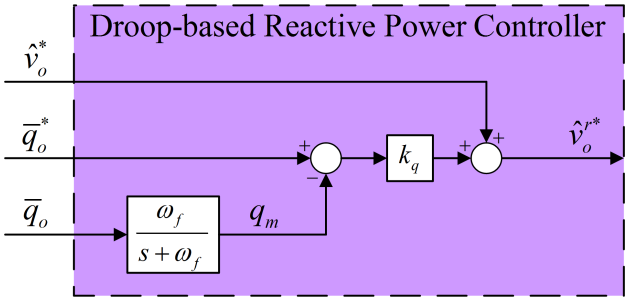

Fig. 6. Reactive power droop controller

it could be estimated from the voltage measurement by a frequency tracking algorithm. Indeed, a PLL is used for this purpose as part of the three-phase VSM from [13]. To avoid this voltage-measurement-based grid frequency estimation, a similar damping effect can be obtained by estimating the grid frequency through low-pass filtering of the VSM speed, as shown in Fig. 5 [16]. Indeed, this ensures a simpler implementation and is almost equivalent to grid frequency tracking since the speed of the VSM in grid connected operation will always settle to the grid frequency as long as the system is stable. Moreover, this solution presents advantages when operating in islanded mode since it is independent of the operating conditions.

It should also be noted that there will be a filtering effect in the measured output power feedback signal $\bar{p}_o$ in (8) due to the SOGI-QSGs used for generating the virtual two phase system. However, with the SOGI-QSGs tuned with a gain $k = \sqrt{2}$ according to [21], it is demonstrated in [28] that the filtering effect on the amplitude or on signals in a Synchronous Reference Frame (SRF) can be approximated by a first order low pass filter:

$$h_{SOGI-QSG}(s) \approx \frac{1}{1+T_{SOGI-QSG}^{SRF}\cdot s} \tag{9}$$

The approximated equivalent filtering time constant found by curve fitting in [28] was in the range of a quarter of the fundamental frequency period. Since the inertia constant of a SM usually will be in the range of several seconds, and the VSM is intended to emulate the SM inertial dynamics, this filtering delay will have almost negligible impact on the dynamics of the virtual swing equation.

The reactive power controller applied in this paper is a conventional droop controller similar to what is commonly used in Uninterruptable Power Supply (UPS) systems and microgrids [29]. A block diagram of the implementation is shown in Fig. 6, where it can be seen that the only difference from a traditional three-phase implementation is that the dynamic average value of the reactive power in the single-phase circuit, as estimated from (7), is used as the feedback signal. Similarly as for the active power control, the filtering effect of the reactive power calculation based on the SOGI-QSG output signals will be limited as long as the reactive power droop controller is tuned for relatively slow response.

F. Initialization and grid synchronization

Since the VSM grid synchronization mechanism is based on the power balance of the virtual swing equation, the initialization and start-up procedures of a VSM controlled converter will be different than for PLL-based control systems. Indeed, the power balance of the virtual swing equation cannot be established before the converter is in operation. Therefore, also the VSM speed, which is used to ensure frequency adaptive implementation of the SOGI-QSGs and the PR controllers in the proposed control scheme, will not be available before the VSM power balance is established.

Considering the case where a VSM should start operation for battery charging, the voltage measurement at the filter capacitor will be available as in a PLL-based control. Thus, the grid frequency can be tracked from the outputs of the SOGI-QSG used for processing the voltage measurement, by either a PLL or a Frequency Locked Loop (FLL) [21], [27]. The integrator giving the VSM speed in the virtual swing equation, can then be initialized to the estimated grid frequency $\tilde{\omega}_g$, i.e. by setting $\omega_{VSM,0} = \tilde{\omega}_{g,0}$. At the same time, the VSM phase angle should be initialized to the phase angle of the filter capacitor voltage according to (10), while the initial voltage reference could be set according to (11):

$$\theta_{VSM,0} = \tan^{-1}\left(\frac{v'_{o,\beta,0}}{v'_{o,\alpha,0}}\right) \tag{10}$$

$$\hat{v}_{o,0}^* = \sqrt{v'^{\,2}_{o,\alpha,0} + v'^{\,2}_{o,\beta,0}} \tag{11}$$

The initialization strategy outlined above will be mainly relevant for ensuring smooth startup in grid connected operation. However, it might also be relevant to synchronize a VSM to the grid while continuously feeding a local load. This will require a dedicated synchronization strategy depending on additional voltage measurements and an additional secondary controller, as discussed for a three-phase VSM in [30].

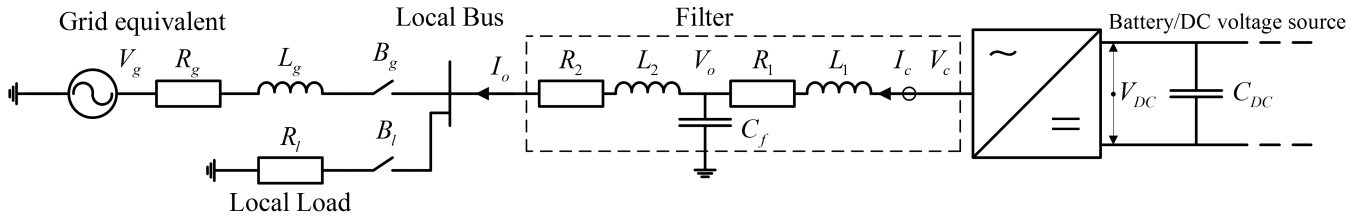

Fig. 7. Overview of system configuration for simulation and experiments

III. Simulations and Experimental Verification

The operation and performances of the single-phase VSM-based control system from Fig. 1 have been investigated by executing both numerical simulations and experimental testing. The overall system configuration used for both the simulations and experiments is shown in Fig. 7, where the VSM-based converter system is connected to a distribution grid and to a local resistive load through contactors B_g and B_l, respectively. Thus, the system can be operated in either grid-connected mode for charging the EV battery while providing V2G services or it can be operated in islanded mode for feeding the local load.

For simplicity, a stiff voltage source has been connected on the dc side of the converter, emulating a simplified behavior of the battery on board of the EV within a short time frame. For practical applications, the State-of-Charge of the battery must be monitored and the provision of ancillary services balanced with the charging requirements [31]. Similarly, the operation in islanded mode must be managed within the allowed discharge of the battery, and possibly balanced with residential generation sources in the islanded system [32]. However, such functions can be significantly slower than the control loops investigated in this paper. Therefore, they can be integrated in a higher hierarchical control layer for power and energy balance management under similar structures as discussed in [33], and will not be further discussed in this paper.

A. System parameters and controller implementation

The main parameters of the investigated system configuration are reported in Table I. The parameters for the simulated system are selected to be the same as for the laboratory setup, with the following exceptions:

- For simplicity and due to limited availability of components, an LC filter is used for the experiments instead of the LCL shown in Fig. 7. This results in $r_2 = l_2 = 0$ in the laboratory setup.
- The equivalent grid impedance given by r_g and l_g is not exactly known in the experimental setup.

The control system has been implemented in Matlab/Simulink and the controller implementation for the laboratory experiments is based on an Opal-RT platform for real-time simulation and rapid prototyping. In the experimental setup, the Opal-RT platform is calculating in real-time the Simulink-based controllers and is generating the PWM signals for the actual converter. Thus, the same Simulink-model for the control system can be used both in simulation and for the experimental verification. All controller functions have been implemented in digital, discrete-time, form with a fixed control time step of 100μs.

TABLE I Parameters of Investigated VSM Configuration

Parameter	Value	Parameter	Value
Rated voltage $V_{g,RMS}$	230 V	Filter inductance l_1	0.08 pu
Rated power S_b	3.3 kVA	Filter resistance r_{l1}	0.01 pu
Rated angular frequency ω_b	2π*50 rad/s	Filter capacitance c_f	0.12 pu
Switching frequency and sampling frequency $f_{sw} = f_{Samp}$	10 kHz	Filter inductance l_2	0.02 pu
VSM Inertia constant T_a	2 s	Filter resistance r_{l2}	0.002 pu
VSM Damping coefficient k_d	200 pu	Grid inductance l_g	0.039 pu
Active power droop gain, k_ω	25 pu	Grid resistance r_g	0.006 pu
Voltage reference $\hat{v}^*$	1.0 pu	Grid voltage $\hat{v}_g$	1.0 pu
Reactive power droop gain, k_q	0.1 pu	Local load, r_l	4.5 pu

The control time-step is equal to the period of the carrier signal used for PWM modulation of the converter, resulting in 10 kHz switching frequency. However, for simplicity and increased speed of simulation an average model is used to represent the converter in the time-domain simulations. The discrete time digital implementation of the SOGI-based frequency adaptive PR controllers is based on a two-integrator scheme with backwards Euler integration for both integrators, accounting for the inherent one-step time delay of the digital signal processing [16], [34]. However, the SOGI-QSGs are implemented according to the state-space approach presented in [35].

B. Overview of investigated cases

In order to investigate the basic functionalities of the VSM-based system, the following two main scenarios have been considered for both simulations and experiments:

1. A step change in the power reference for the battery charger.
2. A sudden disconnection of the external grid resulting in islanding of the charger and the local load.

In addition, the response of the VSM in grid connected mode has been simulated for sudden changes in the grid frequency and in the grid voltage phase angle.

C. Response to step in power reference

In normal operation, the system is operating in grid-connected mode and the VSM-controlled converter is charging the battery with power from the grid. Unlike conventional chargers, the power absorbed from the grid is not necessarily regulated exactly to the set-point coming from the battery controller since the charging power can be slightly modified by the droop controller of the VSM for participating in the primary frequency regulation of the grid.

An example showing the behavior of the simulated system in response to a step in the active power reference from zero

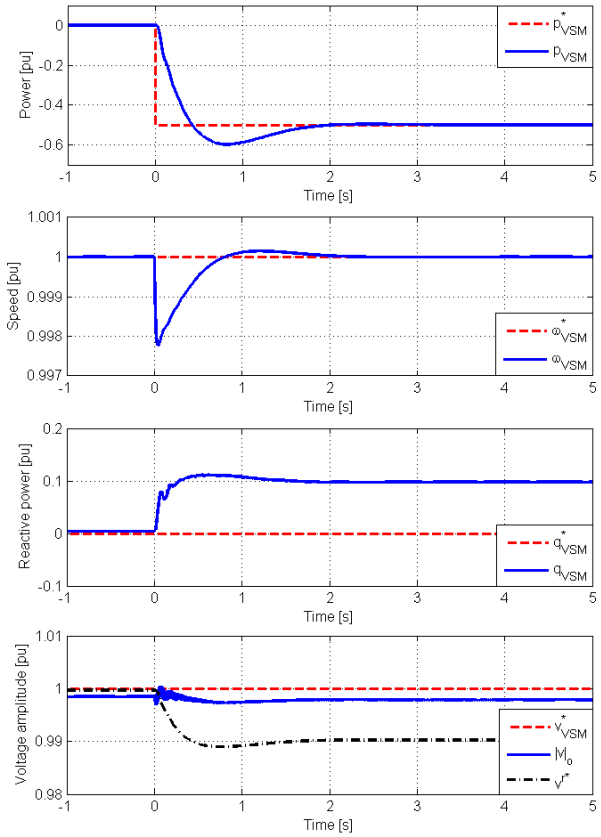

Fig. 8. Simulation results; response in average power flow, virtual inertia speed, reactive power flow and voltage amplitude for the VSM-controlled converter when exposed to a step in power reference

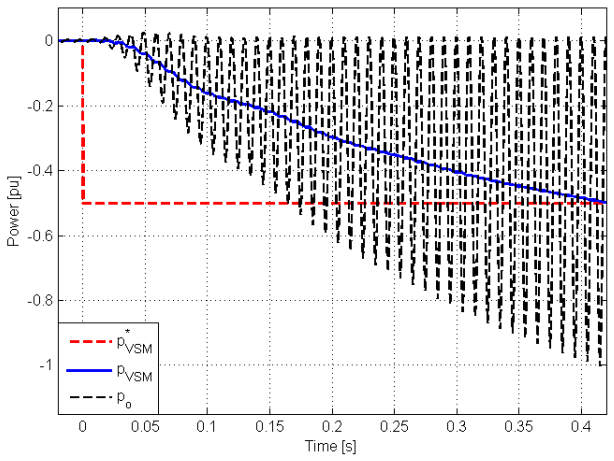

Fig. 9. Simulation results; response in average power and instantaneous power flow of the single-phase VSM to a step in power reference

to −0.5 p.u (EV charging) is shown in Fig. 8. It can be noticed that both power and frequency responses resemble the dynamics of a well-damped SM subject to a disturbance or change of operating conditions. Moreover, it can be observed that the steady state frequency of the VSM remains equal to the grid frequency, regardless of the load. In the simulation, the grid frequency is constant and equal to the nominal value; therefore, the droop function of the VSM is inactive and the charging power delivered to the battery is exactly equal to the commanded value.

The active power feedback signal ($p_{VSM} = \bar{p}_o$) to the VSM swing equation as shown in Fig. 8 is clearly free from double

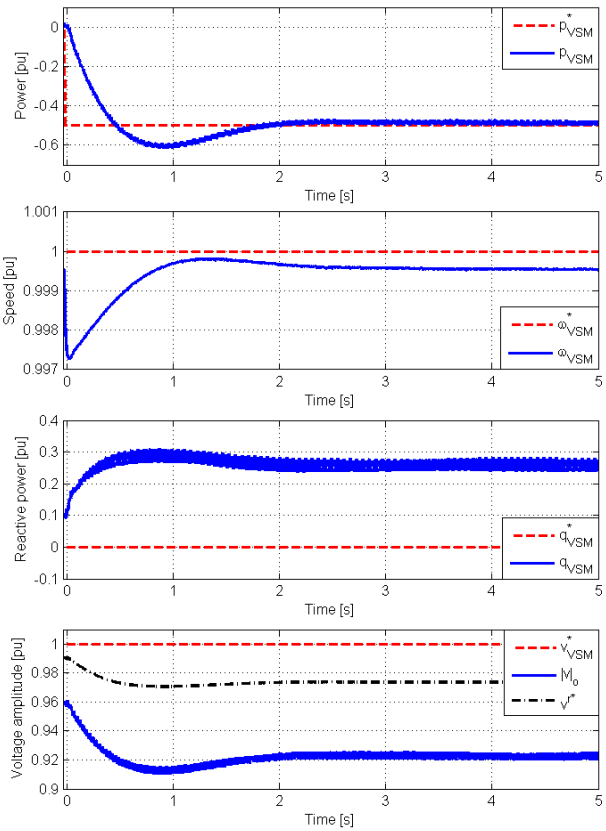

Fig. 10. Experimental results; step in power reference from 0 to −0.5 pu when operating in grid connected battery-charging mode

frequency oscillations in steady state, as expected from the applied method for calculating the average active and reactive power flow. An enlarged view of the power transient following the step is depicted in Fig. 9, where the benefits of the virtual two-phase approach can be easily appreciated by observing the oscillations present in the instantaneous active power p_o flowing in the circuit against the smooth active power p_{VSM} ($= \bar{p}_o$) applied to the virtual inertia

From the two lower plots in Fig. 8 it can also be seen that the grid voltage amplitude ($|v|_0 = \hat{v}_o$) changes slightly with the load due to the grid impedance present in the system. Therefore, the VSM participates in the voltage regulation process by injecting reactive power to the grid when more active power is absorbed. From the figure, it can also be seen how the internal voltage amplitude reference ($v^{r*} = \hat{v}_o^{r*}$) behind the virtual impedance is changing more with the load than the actual output voltage amplitude. This effect is helping to stabilize the voltage control loop in case of strong grid conditions where the EV charger will not be able to influence the grid voltage.

The same step in charging power reference has been imposed on the experimental setup, with results shown in Fig. 10. The system response in terms of active power flow and VSM inertial dynamics can be seen to be almost identical to the simulated case. The only noticeable difference between the two cases is that the actual grid frequency was not exactly equal to the nominal value during the experiments. However, the difference is so small that the effect of the active power droop is barely noticeable and the charging power is practically equal to its set-point. The

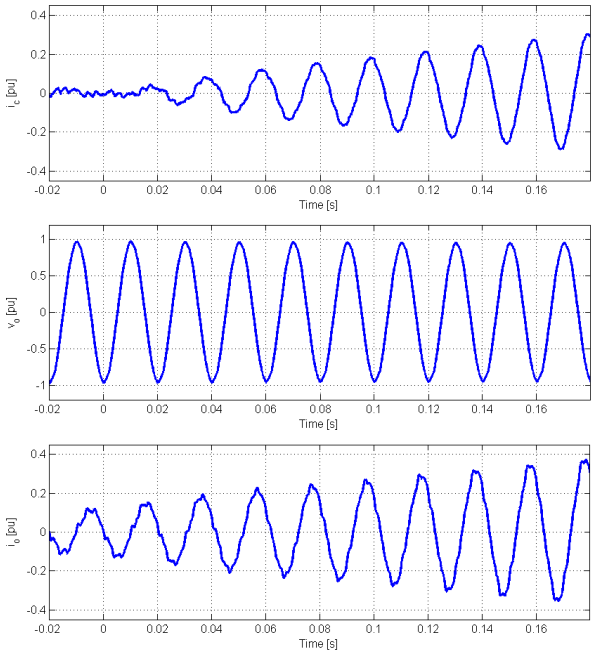

Fig. 11. Experimental results; step in power reference from 0 to −0.5 pu when operating in grid connected battery-charging mode

response in reactive power and voltage amplitude is similar in nature to the simulated case; however, due to the different grid impedance and the different filter configurations the voltage is varying much more with increasing active power flow compared to the simulated case, resulting in increased reactive power contribution from the VSM in an attempt to support the weak grid.

An enlarged view of the instantaneous currents i_c and i_o and the filter capacitor voltage v_o for the initial system response is reported in Fig. 11, showing the smooth behavior of the system following the abrupt change in power set-point. From the current waveforms it can also be noticed that there is a small harmonic distortion in the system resulting from background distortion in the grid voltage.

D. Simulated response to changes in grid frequency and phase angle

To demonstrate the response of the VSM to changes in the grid frequency, a sudden reduction of grid frequency to 49.8 Hz, corresponding to a step of –0.004 pu, has been simulated when the VSM is operated for battery charging with a power reference of –0.5 pu. For a real power system, the frequency will never change instantaneously, but this case is simulated as a worst case to demonstrate the inertial behavior of the VSM. The response in average power and in VSM speed is shown in Fig. 12. From this figure it can be seen how the reduction in grid frequency is releasing inertial energy from the VSM, resulting in a transient reduction of the charging power, including a short period with power injection back to the grid. However, the transient is smooth and well damped, and the VSM settles to a new operating condition corresponding to the reduced grid frequency. Thus, the charging power is also reduced to –0.4 pu after the transient, according to the frequency droop gain of 25 pu.

The VSM has also been simulated with a sudden step of grid voltage phase angle of –7.5°, and the resulting response

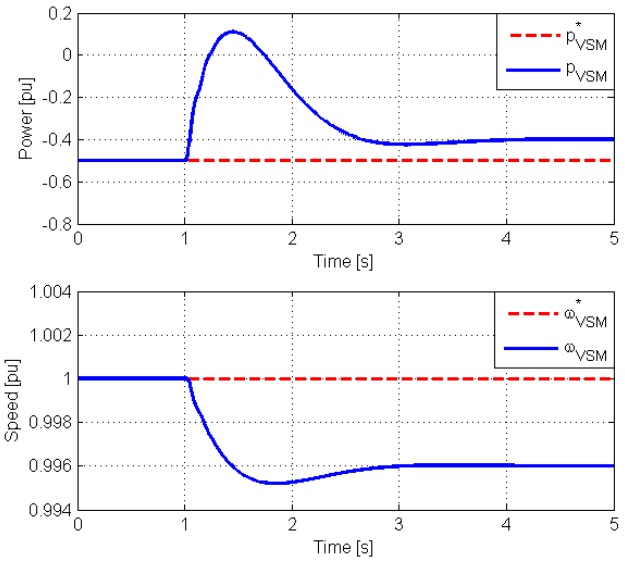

Fig. 12. Simulation results showing the VSM response to a step of –0.004 pu in the grid frequency

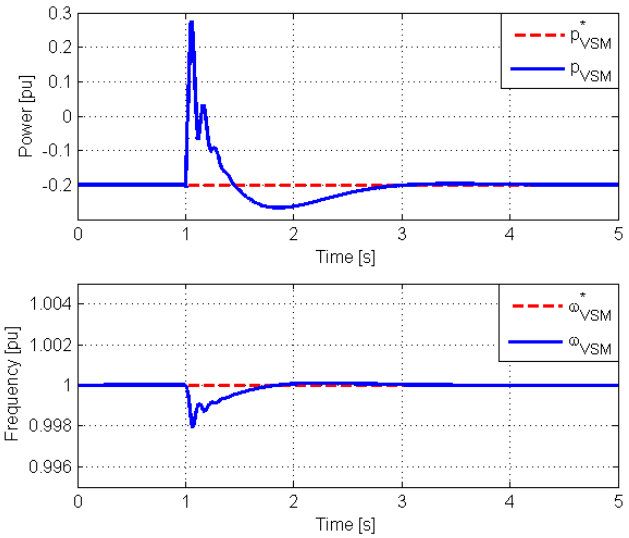

Fig. 13. Simulation results showing the VSM response to a step of –7.5° in grid voltage phase angle

in average power and VSM speed is shown in Fig. 13. In this case, the system is simulated with a charging power of –0.2 pu before the transient. Due to the sudden reduction of grid voltage phase angle, the VSM is again releasing inertial energy by reducing its charging power and feeding power back to the grid for a short period of time, which is also reflected in a small drop in the VSM speed. Since the phase angle step is causing an instantaneous change of equivalent grid voltage, the LC filter dynamics and the controller dynamics of the VSM are also excited, but it can be seen from the figure that the corresponding dynamics are quickly damped. After the initial transient, a clear inertial response of the VSM can be observed when the virtual swing equation is recovering some of the energy it was releasing in the beginning of the transient. However, since the VSM has a high internal damping, both the power and the virtual speed are settling smoothly.

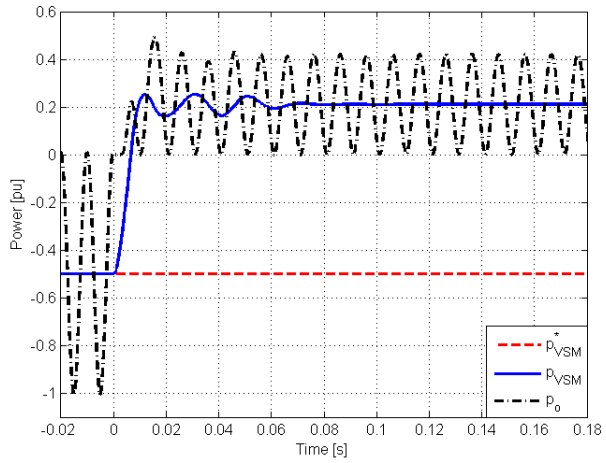

Fig. 14. Simulation results; power responses of the VSM to a sudden islanding condition with reversed power flow

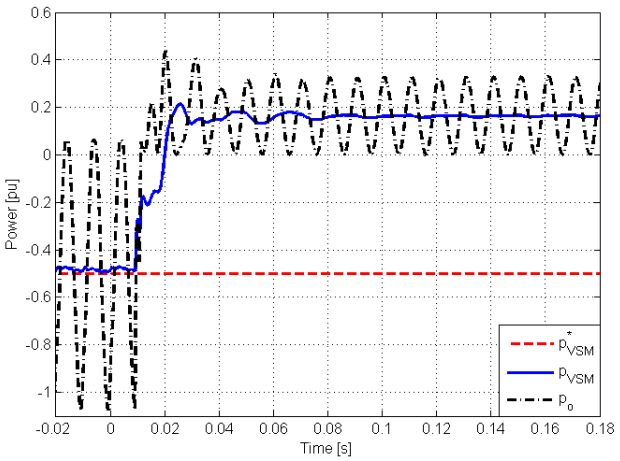

Fig. 16. Experimental results: power responses of the VSM to a sudden islanding condition with reversed power flow

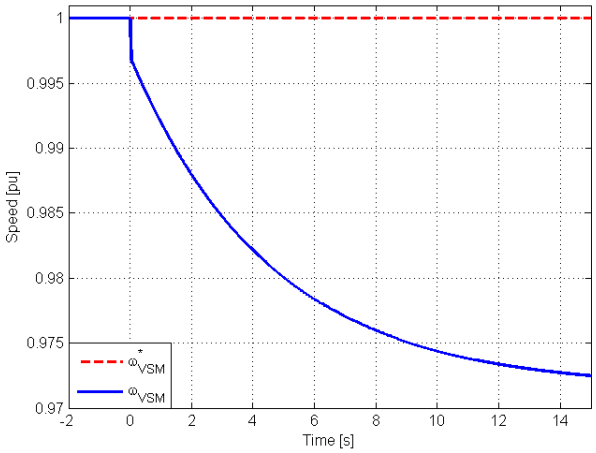

Fig. 15. Simulation results; response in VSM speed to a sudden islanding condition with a local load

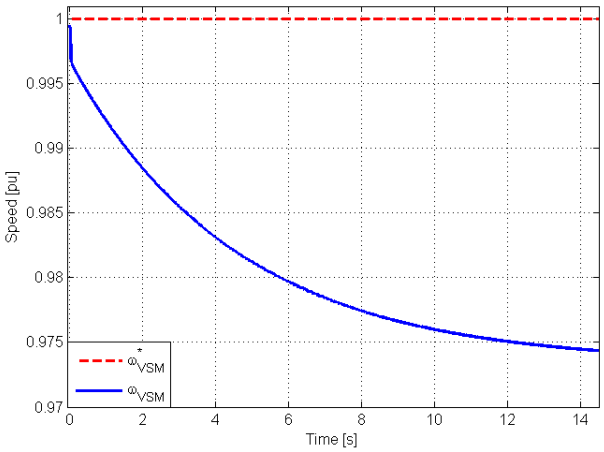

Fig. 17. Experimental results: response in VSM speed to a sudden islanding condition with a local load

E. Response to sudden islanding conditions

The proposed VSM-based control system is inherently capable of islanded operation like a traditional SM. Thus, with such a control system it is possible to use the battery of an EV as a back-up power supply (UPS) for a local load like a single household in case of power system blackouts. To illustrate this feature, the system from Fig. 7 is simulated for the case when the breaker connecting the local bus to the main grid is opened while the EV was being charged. The main results are shown in Fig. 14 and Fig. 15. From Fig. 14 it can be seen that the system quickly and seamlessly commutates from EV charging mode into UPS mode, supplying the required 0.2 p.u. of power to the local load. The speed of the VSM during the transition is shown in Fig. 15, illustrating how the isolated local grid is smoothly settling to operate at a frequency lower than nominal (0.972 p.u. in this case), according to the active power droop gain.

The same behavior is reproduced with the experimental setup, as shown in Fig. 16 and Fig. 17. Again, the only noticeable difference between simulations and experiments is given by a slightly higher reactive power contribution of the VSM-based converter prior to islanding, due to the higher equivalent grid impedance. There is also a small difference in power during the islanded conditions, mainly due to different reactive power flow and corresponding differences in actual load voltage.

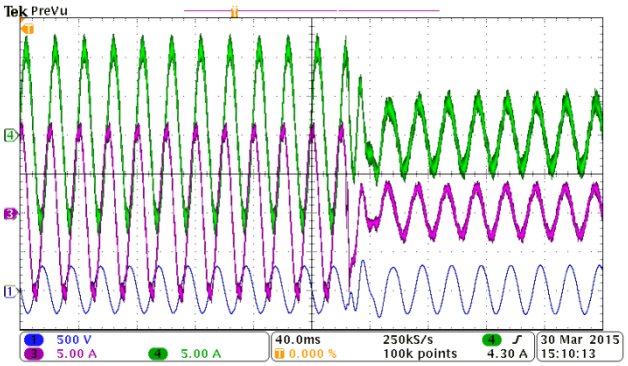

Fig. 18. Measured values of converter current (green), grid side current (purple) and capacitor voltage (blue) in response to sudden islanding

A screenshot of the voltage and current transients resulting from sudden islanding was taken with a digital oscilloscope and is reported in Fig. 18. Apart from a noticeable distortion associated with the transient resulting from arching during the breaker operation, the transition is quite smooth. As expected from the instantaneous power flow plotted in Fig. 16 all the electrical quantities quickly settle to the new steady-state with no dangerous overcurrent or overvoltage.

IV. Conclusion

This paper has presented a control system implementation for a single-phase Virtual Synchronous Machine (VSM). The investigated control system has been demonstrated by simulations and experimental verifications to be capable of providing ancillary services like participation in primary frequency control, inertia emulation for contribution to the spinning reserve and local voltage or reactive power regulation. The proposed implementation also has the inherent capability for feeding local loads in islanded operation. Thus, the VSM-based control approach can be a suitable option for providing Vehicle-to-Grid (V2G) services from domestic single-phase battery chargers for Electric Vehicles. The same control approach can also be used for any other energy storages or small scale distributed generation systems with single-phase grid interface

References

[1] The Information Council for Road Traffic in Norway, National sales statistics for 2015, available from: http://www.ofvas.no/bilsalget-i-oktober/category641.html

[2] J. A. P. Lopes, F. J. Soares, P. M. R. Almeida, "Integration of Electric Vehicles in the Electric Power Systems," in *Proceedings of the IEEE*, Vol. 99, No. 1, January 2011, pp 168-183

[3] M. Yilmaz, P. T. Krein, "Review of the Impact of Vehicle-to-Grid Technologies on Distribution Systems and Utility Interfaces," in *IEEE Transactions on Power Electronics*, Vol. 28, No. 12, December 2013, pp. 5673-5689

[4] K. M. Tan, V. K. Ramachandaramurthy, J. Y. Yong, "Integration of electric vehicles in smart grid: A review on vehicle to grid technologies and optimization techniques," in *Renewable and Sustainable Energy Reviews*, Vol 53, January 2016, pp. 720-732

[5] I. Cvetkovic, T. Thacker, D. Dong, G. Francis, V. Podosinov, D. Boroyevich, F. Wang, R. Burgos, G. Skutt, J. Lesko, "Future Home Uninterruptible Renewable Energy System with Vehicle-to-Grid Technology," in *Proceedings of the 2009 IEEE Energy Conversion Congress and Exposition*, ECCE 2009, San Jose, California, USA, 20-24 September 2009, pp. 2675-2681

[6] B. Liu, K. T. Chau, D. Wu, S. Gao, "Opportunities and Challenges of Vehicle-to-Home, Vehicle-to-Vehicle, and Vehicle-to-Grid Technologies," in *Proceedings of the IEEE*, Vol. 101, No. 11, November 2013, pp. 2409-2427

[7] J. García-Villalobos, I. Zamora, J. I. San Martín, I. Junquera, P. Eguía, "Delivering Energy from PEV batteries: V2G, V2B and V2H approaches," in *Proceedings of the International Conference on Renewable Energies and Power Quality*, ICREPQ'15, La Coruña, Spain, 25-27 March 2015, 6 pp.

[8] H.-P. Beck, R. Hesse, "Virtual Synchronous Machine," in *Proceedings of the 9th International Conference on Electrical Power Quality and Utilisation*, Barcelona, Spain, 9-11 October 2007, 6 pp.

[9] Y. Chen, R. Hesse, D. Turschner, H.-P. Beck, "Dynamic Properties of the Virtual Synchronous Machine (VSIMA)" in *Proceedings of the International Conference on Renewable Energies and Power Quality*, ICREPQ'11, Las Palmas, Spain, 13-15 April 2011, 5 pp.

[10] K. Visscher, S. W. H. De Haan, "Virtual Synchronous Machines (VSG's) for Frequency Stabilization in Future Grids with a Significant Share of Decentralized Generation," in *Proceedings of the CIRED seminar 2008: SmartGrids for Distribution*, Frankfurt, Germany, 23-24 June 2008, 4 pp.

[11] Q.-C. Zhong, G. Weiss, "Synchronverters: Inverters That Mimic Synchronous Generators," *IEEE Transactions on Industrial Electronics*, vol. 58, no. 4, April 2011, pp. 1259-1267

[12] S. D'Arco, J. A. Suul, "Virtual Synchronous Machines – Classification of Implementations and Analysis of Equivalence to Droop Controllers for Microgrids," in *Proceedings of IEEE PowerTech Grenoble 2013*, Grenoble, France, 16-20 June 2013, 7 pp.

[13] S. D'Arco, J. A. Suul, O. B. Fosso, "A Virtual Synchronous Machine Implementation for Distributed Control of Power Converters in SmartGrids," in *Electric Power System Research*, Vol. 122, May 2015, pp. 180-197

[14] C. Pelczar, "*Mobile Virtual Synchronous Machine for Vehicle-to-Grid* Applications," Dr. Ing. Dissertation, Clausthal University of Technology, 2012

[15] T. K. Vrana, C. Hille, "A novel control method for dispersed converters providing dynamic frequency response," in *Electrical Engineering*, Vol. 93, No. 4, December 2011, pp 217-226

[16] J. A. Suul, S. D'Arco, G. Guidi, "A Single-Phase Virtual Synchronous Machine for Providing Vehicle-to-Grid Services from Electric Vehicle Battery Chargers," in *Proceedings of the International Electric Vehicle Technology Conference & Automotive Power Electronics*, EVTeC & APE Japan, Yokohama, Japan, 22-24 May 2014, 7 pp.

[17] W. Jiang, Z. Lv, Q. Zhong, B. Zeng, G. Li, "Virtual Synchronous Motor Based Control Scheme of Electric Vehicle Charger," in *Proceedings of the 2014 International Conference on Power System Technology*, POWERCON 2014, Chengdu, China, 20-22 October 2014, pp. 2686-2692

[18] Z. Zeng, R. Zhao, H. Yang, C. Cheng, S. Tang, "Single-Phase Virtual Synchronous Generator for Distributed Energy Sources," in *Proceedings of the 2013 International Conference on Electrical Machines and Systems*, ICEMS 2013, Busan, Korea, 26-29 October 2013, pp. 190-195

[19] J. A. Suul, S. D'Arco, G. Guidi, "Virtual Synchronous Machine-based Control of a Single-phase Bi-directional Battery Charger for Providing Vehicle-to-Grid Services," in *Proceedings of the 9th International Conference on Power Electronics* – ICPE 2015-ECCE Asia, Seoul, Korea, 1-5 June 2015, 8 pp.

[20] X. Yuan, W. Merk, H. Stemmler, J. Almelling, "Stationary-Frame Generalized Integrators for Current Control of Active Power Filters with Zero Steady-State Error for Current Harmonics of Concern Under Unbalanced and Distorted Operating Conditions," in *IEEE Transactions on Industry Applications*, Vol. 38, No. 2, March/April 2002, pp. 523-532

[21] P. Rodriguez, R. Teodorescu, I. Candela, A. V. Timbus, M. Liserre, F. Blaabjerg, "New Positive-Sequence Voltage Detector for Grid Synchronization of Power Converters Under Faulty Grid Conditions," *in Proceedings of the 37th Annual IEEE Power Electronics Specialists Conference*, PESC'06, Jeju, Korea, 18-22 June 2006, 7 pp.

[22] D. N. Zmood, D. G. Holmes, G. H. Bode, "Frequency-Domain Analysis of Three-Phase Linear Current Regulators," in *IEEE Transactions on Industry Applications*, Vol. 37, No. 2, March/April 2001, pp. 601-610

[23] C. Bajracharya, M. Molinas, J. A. Suul, Tore M. Undeland: "Understanding of tuning techniques of converter controllers for VSC-HVDC," in *Proceedings of Nordic Workshop on Power and Industrial Electronics*, NORPIE 2008, Espoo, Finland, 9-11 June, 2008, 8 pp.

[24] S. D'Arco, J. A. Suul, O. B. Fosso, "Automatic Tuning of Cascaded Controllers for Power Converters using Eigenvalue Parametric Sensitivities," in *IEEE Transactions on Industry Applications*, Vol. 51, No. 2, March/April 2015, pp. 1743-1753

[25] W. Yao, M. Chen, J. Matas, J. M. Guerrero, Z.-M. Qian, "Design and Analysis of the Droop Control Method for Parallel Inverters Considering the Impact of the Complex Impedance on the Power Sharing," in *IEEE Transactions on Industrial Electronics*, Vol. 58, No. 2, February 2011, pp. 576-588

[26] J. Matas, M. Castilla, L. G. de Vicuña, J. Miret, J. C. Vasquez, "Virtual Impedance Loop for Droop-Controlled Single-Phase Parallel Inverters Using a Second-Order General-Integrator Scheme," in *IEEE Transactions on Power Electronics*, Vol. 25, No. 12, December 2010, pp. 2993-3002

[27] R. Teodorescu, M. Liserre, P. Rodríguez, "*Grid Converters for Photovoltaic and Wind Power Systems*," IEEE / John Wiley & Sons, Chichester, UK, 2011

[28] S. Danielsen; O. B. Fosso; M. Molinas; J. A. Suul; T. Toftevaag: "Simplified models of single-phase power electronic inverter for railway power system stability analysis – Development and evaluation," *Electric Power System Research*, Vol. 80, No. 2, February 2010, pp. 204-214

[29] J. Rocabert, A. Luna, F. Blaabjerg, P. Rodríguez, "Control of Power Converters in AC Microgrids," in *IEEE Transactions on Power Electronics*, Vol. 27, No. 11, November 2012, pp. 4734-4749

[30] S. D'Arco, J. A. Suul, "A Synchronization Controller for Grid Reconnection of Islanded Virtual Synchronous Machines," in *Proceedings of the IEEE 6th International Symposium on Power*

Electronics for Distributed Generation, PEDG 2015, Aachen, Germany, 22-25 June 2015, 8 pp.

[31] Y. Ota, H. Taniguchi, T. Nakajima, K. M. Liyanage, J. Baba, A. Yokoyama, "Autonomous Distributed V2G (Vehicle-to-Grid) Satisfying Scheduled Charging," in *IEEE Transactions on Smart Grid*, Vol. 3, No. 1, March 2012, pp. 559-564

[32] D. P. Tuttle, R. L. Fares, R. Baldick, M. E. Webber, "Plug-In Vehicle to Home (V2H) Duration and Power Output Capability," in *Proceedings of the 2013 IEEE Transportation Electrification Conference and Expo: Components, Systems and Power Electronics – From Technology to Business and Public Policy,* Dearborn, Michigan, USA, 16-19 June 2013, 7 pp.

[33] J. M. Guerrero, J. C. Vasquez, J. Matas, L. G. de Vicuña. M. Castilla, "Hierarchical Control of Droop-Controlled AC and DC Microgrids – A General Approach Toward Standardization, in *IEEE Transactions on Industrial Electronics*, vol. 58, no. 1, January 2011, pp. 158-172

[34] F. J. Rodríguez, E. Bueno, M. Aredes, L. G. B. Rolim, F. A. S. Neves, M. C. Cavalcanti, "Discrete-time implementation of second order generalized integrators for grid converters," in *Proceedings of the 34th Annual Conference of the IEEE Industrial Electronics Society*, IECON 2008, Orlando, Florida, USA, 10-13 November 2008, pp.176-181

[35] A. Luna, J. Rocabert, G. Vazquez, P. Rodríguez, R. Teodorescu, F. Corcoles, "Grid Synchronization for Advanced Power Processing and FACTS in Wind Power Systems," in *Proceedings of the 2010 IEEE Symposium on Industrial Electronics*, ISIE 2010, Bari, Italy, 4-7 July 2010, pp. 2915-2920

Jon Are Suul (M'11) received the M.Sc. and PhD degrees from the Department of Electric Power Engineering at the Norwegian University of Science and Technology (NTNU), Trondheim, Norway, in 2006 and 2012, respectively.

From 2006 to 2007, he was with SINTEF Energy Research, Trondheim, where he was engaged in simulation of power electronic systems until starting his PhD studies. In 2008, he was a guest Ph.D. student for two months with the Energy Technology Research Institute of the National Institute of Advanced Industrial Science and Technology, Tsukuba, Japan. He was also a visiting Ph.D. student for two months with the Research Center on Renewable Electrical Energy Systems, within the Department of Electrical Engineering, Technical University of Catalonia (UPC), Terrassa, Spain, during 2010. Since 2012, he has resumed a part-time position as a Research Scientist at SINTEF Energy Research while also working as a part-time post.doc researcher at the Department of Electric Power Engineering of NTNU. His research interests are mainly related to analysis and control of power electronic converters in power systems and for renewable energy applications.

Salvatore D'Arco received the MSc. and Ph.D. degrees in Electrical Engineering from the University of Naples "Federico II" in 2002 and 2005, respectively.

From 2006 to 2007, he was a post.doc researcher at the University of South Carolina, Columbia, SC, US. In 2008 he joined ASML in The Netherlands as a Power Electronics Designer, where he worked until 2010. From 2010 to 2012 he was a post.doc researcher in the Department of Electric Power Engineering at the Norwegian University of Science and Technology. In 2012 he joined SINTEF Energy Research where he currently works as Research Scientist. He is the author of over 50 scientific papers and he is the holder of one patent. His main research activities are related to control and analysis of power electronic conversion systems for power system applications, including real-time simulation and rapid prototyping of converter control systems.

Giuseppe Guidi (M'00) received the Graduate degree from the University of L'Aquila, L'Aquila, Italy, in 1995, and the Ph.D. degree from the Norwegian University of Science and Technology (NTNU), Trondheim, Norway, in 2009.

He was involved in the field of power electronic drives from 1997 to 2004, joining first Fuji Electric R&D, Japan, as R&D Engineer and then SIEI SpA, Italy, as a Senior Engineer. In 2009, he joined Yokohama National University, Yokohama, Japan, as a Research Associate, working on power converters for electric vehicles. From 2011 he was a part-time Research Associate with NTNU, until joining SINTEF Energy Research, Trondheim, Norway, in 2013. His current research interests include power electronics, traction control, and drive systems for electric propulsion, as well as application of power electronics to renewable energy.